A Multi-Technique Approach for Characterizing the SVN 49 Signal Anomaly Part 1 - Receiver Tracking and IQ Constellation

André Hauschild, Oliver Montenbruck (DLR/GSOC)
Steffen Thölert, Stefan Erker, Michael Meurer (DLR/IKN)
Javad Ashjaee (JAVAD GNSS)

Abstract

The paper presents a characterization of the signal anomaly of SVN 49. A mathematical model is developed to relate the observed multipath to the internal signal reflection. The analyses provided in the paper are based on measurements, which have been collected during a dedicated tracking campaign with a 30m-dish antenna. Data on the L1 and L2 frequency have been collected with four different receivers. In addition, IQ samples have been recorded directly with a spectrum analyzer. The multipath combination of the receiver measurements on L1 and L2 is analyzed to demonstrate the effect of the signal reflections on different correlator spacings. The capability to suppress the signal reflection with receiver's multipath mitigation methods is demonstrated. Finally, a coarse approximation of the attenuation, delay and phase-shift over elevation is obtained from an IQ sample analysis.

Introduction

SVN 49 stands out of the other satellites of the GPS constellation. This space vehicle, which is currently assigned to PRN 1, is a Block IIR-M satellite and has been launched on March 24, 2009, as the second-last of its type. The satellite carries an experimental signal generation payload for the transmission of the L5 signal. The implementation of this feature, which was not foreseen for normal Block IIR-M satellites, became necessary to meet a deadline in frequency utilization set by the International Telecommunication Union (ITU) (Erwin et al. 2009).

After the activation of the signal transmissions, users experienced unexpected residuals of the pseudorange observations on L1 and L2 (Gao et al. 2009, Meurer et al. 2009, Springer and Dilssner 2009). It turned out that the satellite is affected by a signal anomaly and transmits an undesired internal reflection of the L1 and L2 signals in addition to the direct signals. This reflection is created at a filter of the L5 signal generation unit. The impact of this phenomenon on the position and time estimation has been assessed by El-Arini et al. (2010). Komjathy et al. (2010) discuss the effect on group delay and ionosphere slant delay estimation. However, additional studies are expedient for a mathematical description of the problem and the development of a multipath model. This model will help to assess the impact of the signal reflection on the user community.

For this purpose, a tracking campaign to characterize the effect using different techniques has been performed jointly by German Aerospace Center (DLR) and the GPS Wing using DLR's 30 m dish antenna in Weilheim. This paper summarizes the key findings of the campaign in two parts: The first part introduces the mathematical multipath model and the experiment setup for the tracking campaign. An overview of tracking results with four different receivers connected to the high gain antenna is provided. This setup allows studying the impact of the signal reflection on different correlator settings. Additionally, the effect of multipath mitigation techniques, implemented in the different receivers, has been tested. Furthermore, results of the analysis of IQ samples are presented, which allows the estimation of characteristic properties like delay, attenuation and phase of the satellite-induced multipath component of SVN 49.

The second part of the paper will include the reconstruction of the chip shape based on the IQ-samples. The multipath model for the reflected signal from SVN 49 will be parameterized based on these analyses. For validation, the results of the model will be compared to the receiver tracking results from the first part of the paper.

Description and Modeling of the Multipath Reflection

Fig. 1 provides an overview of the transmission chain of the direct and reflected signal for SVN49. The core part is the antenna coupler network, which has the signal generation unit for the L1 and L2 signals connected to the first input port J1. The experimental payload for L5 is connected to the secondary port J2. Part of the signal fed into the J1 port of the antenna coupler leaks out of the J2 port. It enters the cable connecting the L5 signal generation unit, is reflected at the L5 filter and then fed back into the antenna via the second port with an additional geometric cable length of approximately 8 m (Stansell 2009). The direct signal at the J1 port S_{J1} and the reflected signal, which is attenuated, delayed and shifted in phase, at the J2 port S_{J2} are illustrated in Fig. 1.

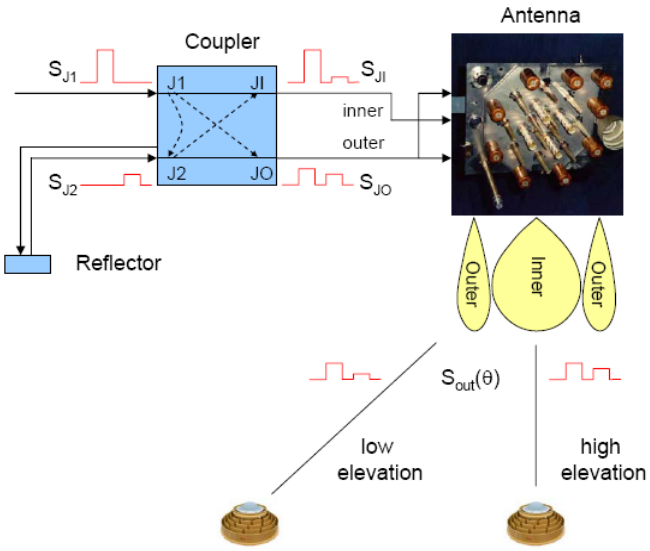

Fig. 1: Schematic of the signal transmission chain of the direct and reflected signal on SVN49

The coupler network distributes the signal power to the twelve antenna elements, which are grouped in two rings: an inner ring with four and an outer ring with eight elements. The inner ring transmits most of the power from the first port of the coupler network with a broad pattern. The outer ring transmits the signal with lower power in a focused pattern and with different phase. As a result, the signal power at small boresight angles (or equivalently high elevation angles on the Earth's surface) is reduced in favor of a more uniform distribution for users at high and low boresight angles from the satellite's perspective. The second input port J2 of the coupler network has a reversed power distribution compared to the first port, i.e. more of the power goes to the outer ring with the higher focus and less is transmitted via the inner ring (Stansell 2009). As a result, the reflections of the L1 and L2 signals are attenuated and superimposed with the direct signals at the output port for the inner antenna ring JI as illustrated in Fig. 1. Vice versa, at the output port for the outer ring the attenuated direct signal is superimposed with the reflected signal.

Finally, the user receives a signal S_{OUT}, which is a combination of S_{JI} and S_{JO} and exhibits a dependency on the boresight angle θ or, equivalently, the elevation angle of SVN49. As a result, the reflected signal manifests itself at the users' receiver as a multipath-error, which has a dependency on elevation (Langley 2009).

For the characterization of the signal anomaly, a mathematical model shall be developed in the following. The direct signal $S_{J1,}$ which is fed into the primary connector of the antenna coupler, is written as:

$$S_{J1} = A(t)e^{j\omega t} \tag{1}$$

In this equation, $A(t)$ is the time-dependent amplitude of the signal, ω is the angular frequency and t is the time. The reflected signal, which is fed back into the secondary port J2, is attenuated by a factor α_R, delayed by a time-constant τ_R and shifted by a phase-shift φ_R:

$$S_{J2} = A(t-\tau_R)e^{j\omega(t-\tau_R)+\varphi_R} \tag{2}$$

The received signal S_{OUT} is a superposition of the two previous input signals. It is important to consider that both signals are affected by the antenna coupler network and the transmitting antenna. Thus S_{OUT} depends on the transfer functions H_{J1} and H_{J2} from the primary and the secondary input port to the user antenna on the ground:

$$S_{OUT} = H_{J1}(\theta)S_{J1} + H_{J2}(\theta)S_{J2} \tag{3}$$

H_{J1} and H_{J2} are not constant but have a dependency on the boresight angle θ. The transfer functions can also be expressed as complex exponential functions:

$$H_{J1} = h_{J1}(\theta)e^{j\varphi_{J1}(\theta)} \tag{4a}$$
$$H_{J2} = h_{J2}(\theta)e^{j\varphi_{J2}(\theta)} \tag{4b}$$

In Eq. 4a and 4b, h_{J1} and h_{J2} describe the gain for signals from the primary and secondary input port, respectively, depending on the boresight angle. Similarly, φ_{J1} and φ_{J2} denote the boresight-dependent phase-shifts of the input signals. It is assumed that H_{J1} and H_{J2} do not cause a differential delay of the signal. This assumption is based on the reasoning that a delay between the signal of the inner and outer antenna ring would cause a boresight-dependent (or elevation-dependent) group delay of the received signals, which is not observed for other GPS satellites. Combining the equations 1-4, we find the following expression for S_{OUT}:

$$S_{OUT} = h_{J1}(\theta)A(t)e^{j(\omega t+\varphi_{J1}(\theta))} + h_{J2}(\theta)\alpha_R A(t-\tau_R)e^{j(\omega(t-\tau_R)+\varphi_R+\varphi_{J2}(\theta))} \tag{5}$$

The delay τ, the attenuation α and the phase-shift φ of the reflected signal at the user's end of the signal transmission chain can then be related to the corresponding values α_R, τ_R and φ_R of the reflection inside the satellite:

$$\tau = \tau_R \tag{6a}$$
$$\varphi = \varphi_R + \varphi_{J2}(\theta) - \varphi_{J1}(\theta) \tag{6b}$$
$$\alpha = \alpha_R h_{J2}(\theta)/h_{J1}(\theta) \tag{6c}$$

Measurements of the antenna gain and phase shift for the L1 frequency as functions of the boresight angle have been reported by Ericson at al. (2010), which allows the determination of the characteristic parameters of the internal reflection based on the observed signal on L1.

Experiment Setup

SVN 49 has been tracked using the 30 m dish antenna located at DLR's ground station in Weilheim, Germany, during a campaign from April 8-19, 2010. The signal analysis facility installed in the deep space antenna is routinely used for tests and performance analyses of GNSS satellites (Thölert et al. 2009b). Due to the small beam width of 0.5°, the signals of a single satellite can be tracked with significantly higher gain compared to normal GNSS antennas. Furthermore, multipath reception from ground based reflectors is almost entirely avoided. Thus, apart from signal delays in the ionosphere and troposphere, the measurements are only affected by receiver noise.
The time of the tracking campaign has been coordinated to coincide with a series of high-elevation passes over the tracking antenna in Weilheim. At that point in time, SVN 49 was moved to a new slot in the GPS constellation in the course of the repositioning campaign to achieve better global coverage. This gradual change in the orbit shifted the satellite's ground track over the antenna location from East to West, resulting in a zenith pass on April 15. As a result, SNV 49 could be tracked for more than one week with maximum elevations higher than 89°, which provided a unique opportunity for signal analysis of the signals over the complete range of elevations. The M-code of SVN 49 has been deactivated exclusively for this tracking campaign during April 13-20, 2010. Furthermore, the satellite transmitted unencrypted P-code during this period.

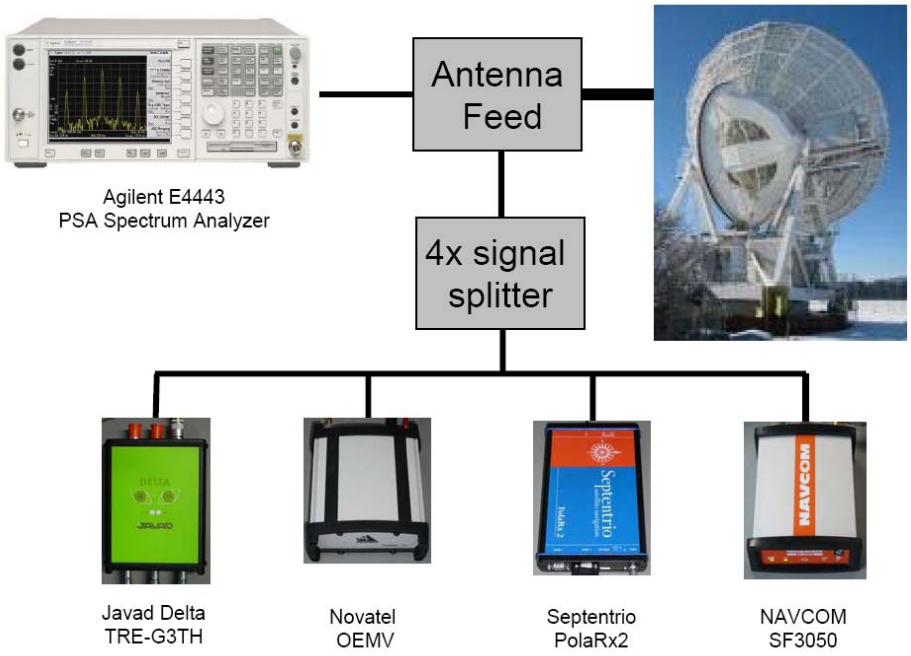

Fig. 2: Experiment setup for SVN49 tracking campaign

The setup of the experiment is depicted in Fig. 1. The measurement equipment is connected to a specially designed antenna feed, which is optimized for the reception of navigation signals in the L-band. IQ-samples of the signals are recorded directly using a spectrum analyzer. For this particular tracking campaign, two Agilent Spectrum Analyzers are used to record samples with a length of 1 second every 15 minutes and 100 milliseconds every 100 seconds.
Additionally, four different receivers are connected to the feed via a passive 4-way signal splitter. A Javad Delta TRE-G3TH (or DG3TH), a NovAtel OEMV, a Septentrio PolaRx2 and

a NavCom SF3050 receiver are used. The receiver's proprietary raw measurements are recorded and then converted into Rinex files, prior to further processing.
All receivers except for the PolaRx2 were operated with dedicated firmware versions, which have been especially designed by the corresponding manufacturers for this tracking campaign. The receivers are configured to use conventional early-minus-late (E-L) correlators for most of the tracking campaign. After the zenith pass, the multi-path mitigation techniques implemented in the different receiver are activated. The Javad receiver tracks the C/A, L2C, P1 and P2 signals of SVN 49 on ten different channels with early-minus-late correlator spacings varying from 0.1 to 1.0 chip. For the tests with the internal multipath-mitigation, the standard firmware version 3.1.5b1 has been used. The NovAtel OEMV receiver tracks C/A and L2C with a conventional 1.0 chip E-L correlator. The Pulse Aperture Correlator (PAC) is used for the tests with multipath mitigation (Jones et al. 2004). In this test, the receiver was also configured to track P2 signals. The NavCom receiver tracks GPS C/A, P1, L2C and P2 signals with a Hatch-correlator, which offers improved multipath-resistance compared to conventional correlators (Hatch et al. 2007). Finally, the Septentrio receiver is operated with a standard firmware for the entire period. The receiver provides C/A-code measurements based on a 1/30 chip early-late correlator for C/A-code. For P1 and P2, the correlator spacing is 2/3 of a chip. The "A Posteriori Multipath Estimator" (APME) is activated for tracking with multipath mitigation (Sleewaegen and Boom 2001). The receiver information is summarized in Tab 1. Even though some of the receivers support tracking of the L5 signal as well, the analysis in this paper is limited to the signals on L1 and L2.

Table 1: Overview of receivers and correlators used in the tracking campaign

Receiver	**Firmware**	**Correlator settings**	
		conventional tracking	**multipath mitigation**
Javad Delta TRE-G3TH	3.2.0b3_tstprn1	0.1…1.0 chip E-L	mpnew (standard firmware 3.1.5b1)
NovAtel OEMV	3.700S30	1.0 chip E-L	PAC correlator
NavCom SF3050	SVN49testmode	-	Hatch correlator
Septentrio PolaRx2	2.6.0-dlr1	C/A: 1/30 chip E-L P(Y): 2/3 chip E-L	APME

Receiver Measurements with a High-Gain Antenna

Prior to the discussion of the tracking results, the processing and analysis strategy shall be explained here in further details. As already mentioned, the raw measurements of each receiver are converted into Rinex files. Next, the 1 Hz observations are smoothed with a Hatch filter with 50 s smoothing interval and decimated to 10 second steps. The pre-processing step has been done for each receiver irrespective of the fact that some receivers have already applied internal smoothing. The combined effect of pseudorange multipath and receiver noise on a signal can be assessed from the difference of code and carrier-phase observations from the corresponding signal, which is corrected for the ionospheric-delay using a carrier-phase measurement from a second frequency. This combination is generally referred to as the multipath-combination and implies the assumption that the carrier-phase multipath is negligible compared to the pseudorange multipath. The multipath combination for a single epoch can be computed from (Kee and Parkinson 1994):

$$MP(\rho_A) = \rho_A - \Phi_A - 2\frac{f_B^2}{f_A^2 - f_B^2}(\Phi_A - \Phi_B) + b_A .$$

In this equation, A and B are the two signals involved and f_A and f_B are the corresponding frequencies. The pseudorange and carrier-phase observables are denote ρ and Φ, respectively. The result of the equation depends on the pseudorange multi-path errors and receiver noise, but is also offset by an arbitrary bias b due to the carrier-phase ambiguities and code delays. To achieve comparable results for the different receivers, this arbitrary offset must be removed in a consistent manner. According to Stansell (2010), the gain pattern of the signal fed into the secondary port of the antenna coupler has a null at an elevation angle of approximately 40° and reverses its polarity at this point. For L2, the null in the gain pattern of the secondary port appears at approximately 30°. Therefore, the multipath plots for L1 and L2 have been aligned to zero at 40° and 30° elevation, respectively.
In addition to the alignment of the offset, a second correction has been applied to remove a trend in the multipath combination over time, which appears to be linear to first approximation. This slope was found to be present in data from all receivers and has a magnitude of a few centimeters per hour. The effect corresponds to a divergence of the pseudorange and carrier-phase over time and leads to a mismatch of the ascending and descending part of the multipath curve if plotted over elevation. This effect could not only be observed for SVN62, but also for SVN57, a Block IIR-M satellite launched in December 2008, which has been tracked as a reference. This divergence is usually not visible in the multipath combination with data from a normal GNSS antenna. A conclusive explanation for this phenomenon is difficult to find at this stage. The slope shows a significant variation from day to day. The Javad, NovAtel and NavCom receivers seem to exhibit similar slopes on the same days, whereas the Septentrio receiver differs significantly. Code- or phase-delay variations in the receiver or the transmitter (or a combination of both) are a possible explanation for this effect. It should be noted that code- and phase-variations of delays common for all satellites in the receiver would not affect “normal” receiver operation, as they are entirely absorbed in the satellite clock solution during positioning. The slope has been removed empirically by fitting a first-order polynomial through the multipath combinations for the C/A-code below 30° elevation. This correction has then been applied as correction not only to the C/A-code, but also all other signals on L1 and L2.

Multipath characteristics for normal E-L correlators

We start the discussion with an overview of the results for the Javad DG3TH, the NovAtel OEMV and the Septentrio PolaRx2 receivers using “conventional” early-late correlators. The multipath combinations for different signals are shown in Fig. 2. All measurements stem from a satellite pass on April 12, 2010, with the exception of the OEMV measurements for P-code on L2, which were recorded on April 16. The two upper plots depict the multipath combination for C/A-code and P-code on L1. It becomes obvious, that the C/A multipath curve starts with a negative offset of approximately 0.10 m for the PolaRx and 0.25 m for the other receivers. For elevations higher than 30°, the multipath curve starts to rise and reaches a maximum at zenith. It amounts to 1.7 m for the Javad DG3TH and the OEMV with 1.0 chip correlator width. As expected, the multipath effect is smaller for smaller correlator spacing: for the Javad DG3TH with 0.1 chip spacing, the maximum effect is 1.5 m and for the PolaRx2 with the smallest correlator width of $1/30^{th}$ of a chip, it amounts to only 1.25 m. A similar picture can also be found for the P-code in the upper right plot. The DG3TH with 1.0 chip correlator spacing and the PolaRx2 with 0.6 chip spacing yield comparable results with 1.5 m for the maximum elevation. The DG3T with 0.1 chip spacing exhibits a reduction of the reflection to 1.25 m.
The plots for the signals on the L2 frequency show a significantly different elevation dependency. At low elevations, the lower left plot for the L2C signal starts at approximately 0.2 m for all receivers and reaches a minimum of about -0.4 m at 65° elevation. At zenith, the

multipath reflection amounts to approximately -0.25 m. For the OEMV and the DG3TH with 1.0 chip correlator width, the L2C signal is significantly noisier than all other signals. A small reduction of the multipath effect can be recognized for the Javad receiver with the narrow correlator. The results for the P-code on L2 in the lower right plot do not differ significantly apart from the lower noise. However, the OEMV receiver exhibits a particular tracking behavior at low elevations. Note that the data for this receiver stems from April 16, when the PAC correlator has been configured to track P-code signals. Closer review of the measurements from this day reveals a very similar tracking behavior of other receivers for P-code on L2 as well. This observation suggests that the unexpected variations are not caused by the OEMV receiver. A more likely explanation is signal interference on this particular day.

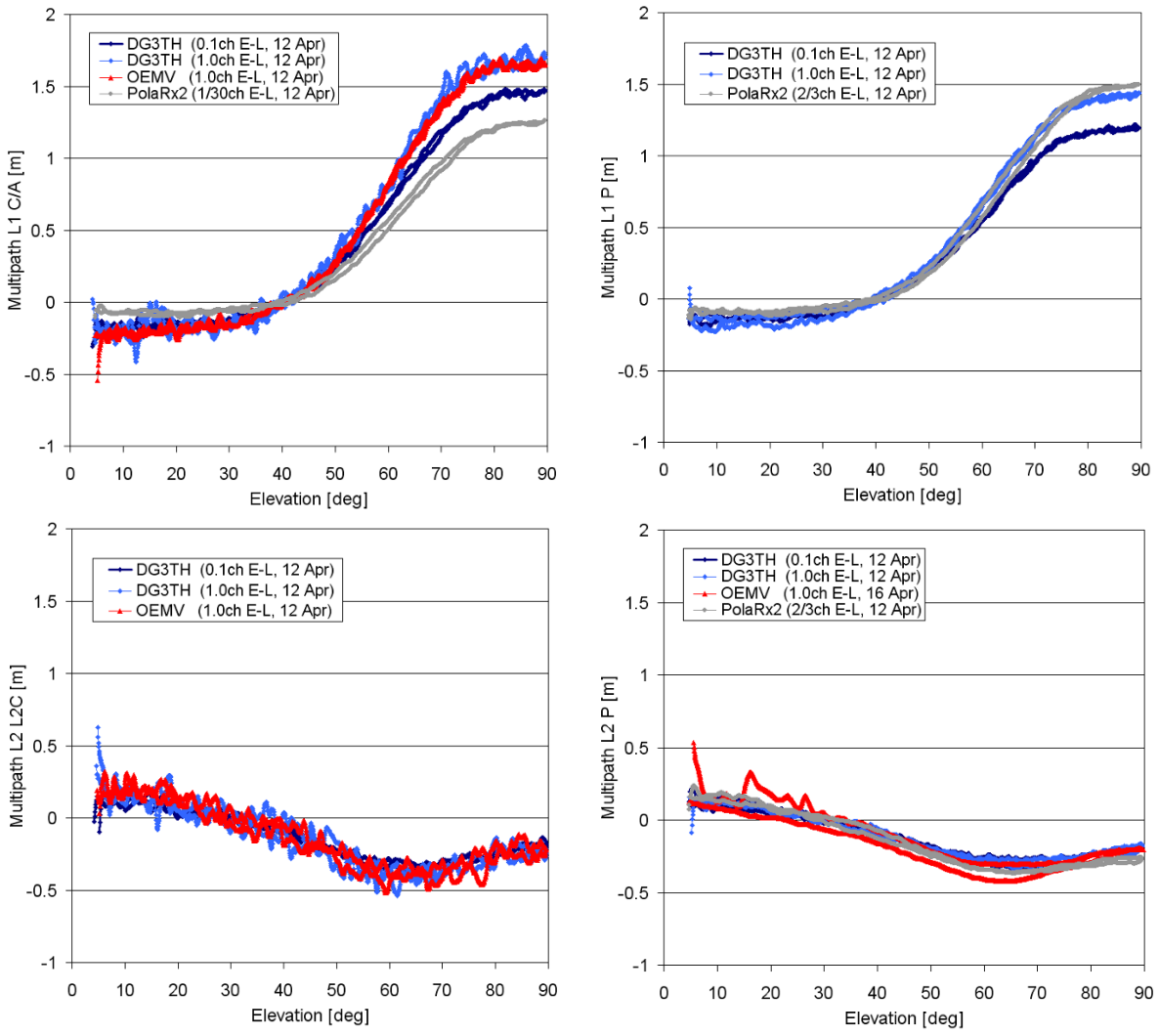

Fig. 3: Multipath over Elevation for L1 C/A-code (upper left plot), L1 P-code (upper right plot), L2C-code (lower left plot) and L2 P-code (lower right plot) for the Javad DG3TH, the NovAtel OEMV and the Septentrio PolaRx2 receiver for April 12, 2010. Note that the PolaRx2 does not provide L2C measurements. The L2 P-code measurements from the OEMV stem from the PAC correlator, which has been configured for tracking on April 16.

Having presented the effect of the signal reflection on different observables, its repeatability shall be discussed in the following. Fig. 3 depicts the results of the multipath combination for the C/A-code for OEMV receiver for 5 days from April 10 until April 19. The plot shows a reasonable consistency for April 12, 14 and 15. All three curves are close together over the complete range of elevations. The plot for April 19 exhibits deviations especially at higher elevations where the ascending and descending part diverge. A similar effect but with larger

magnitude can also be observed for the first day of the test interval. These differences in the multipath combination can either be a receiver-dependent or a satellite-dependent effect.

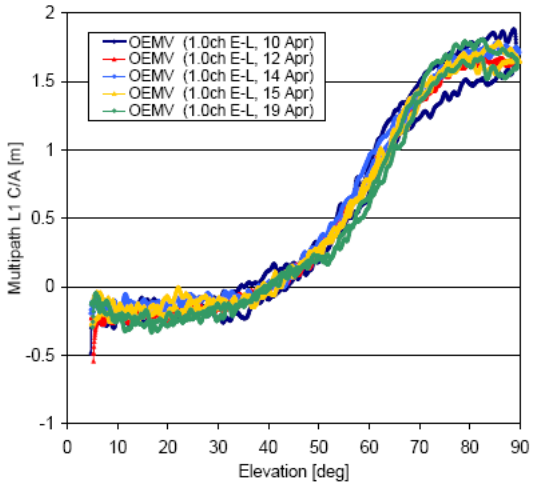

Fig. 4: Daily repeatability of the multipath effect over a period of 9 days from April 10 to April 19, 2010. The plot depicts the results for the multipath combination of the C/A-code signal for the OEMV receiver.

Overview of multi-path mitigation methods

Finally, the results for correlators with special multi-path mitigation feature shall be presented. Again, we limit the discussion the results for the C/A-code signals. Fig. 4 depicts results for all four receivers. Tracking data from the Javad, Septentrio and NavCom receivers with multipath mitigation enabled is available for the satellite pass on April 19. The OEMV was operated with the PAC correlator on April 16. It becomes obvious from the plot that the smallest mitigation effect is found for this correlator type. The maximum multipath at 90° elevation still amounts to 1.5 m, which is similar to 0.1 chip E-L correlator of the DG3TH. The PolaRx2 with the “A Posteriori Multipath Estimator” (APME) exhibits a better suppression of the signal reflection, however, at the price of a significant hysteresis effect. The ascending part of the curve is notably flatter than the descending path and the maximum multipath error is shifted from zenith to approximately 80° elevation. The divergence between the ascending and descending part of the pass is caused by the long time constant in the multipath estimator (Sleewagen, priv. comm.), but can also be expected if code-smoothing with a long time constant is applied. The second best mitigation is achieved with the Hatch-correlator of the SF3050 receiver. Due to its robustness towards multipath, it shows less than half of the maximum multipath error compared to a conventional 1.0-chip E-L correlator. Finally, the Javad receiver has been configured with a standard firmware version, which allows the selection of the “mpnew” multipath mitigation. This mitigation technique virtually eliminates the complete signal reflection, leaving only variations in the order of a decimeter.

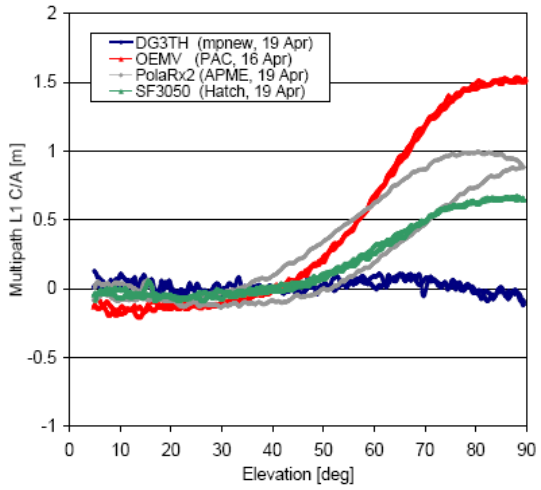

Fig. 5: Tracking results for C/A code with special multipath-mitigation techniques. The plot depicts tracking results for the Javad D3TH with "mpnew"-option, the NovAtel OEMV with PAC correlator, the Septentrio PolaRx2 with APME option and the NavCom SF3050 with Hatch-correlator.

Multipath Characterization from IQ Sample Analysis

After the presentation of the receiver tracking results, the analysis of the recorded IQ samples shall be presented. In this section, characteristic parameters like delay, attenuation and phase-shift of the reflected signal are determined, which will ultimately lead to a development of a complete model for the multipath. This method has been previously described in (Thoelert et al. 2009b) and is based on an iterative fit of simulated and measured IQ constellation diagrams. The left plot in Fig. 5 depicts normalized constellation diagrams for SVN49 at low elevation of 40°, where the reflected signal can be neglected. In direct comparison to the right plot, which shows the diagram at 89° elevation, the change in the diagram caused by multipath becomes clearly visible.

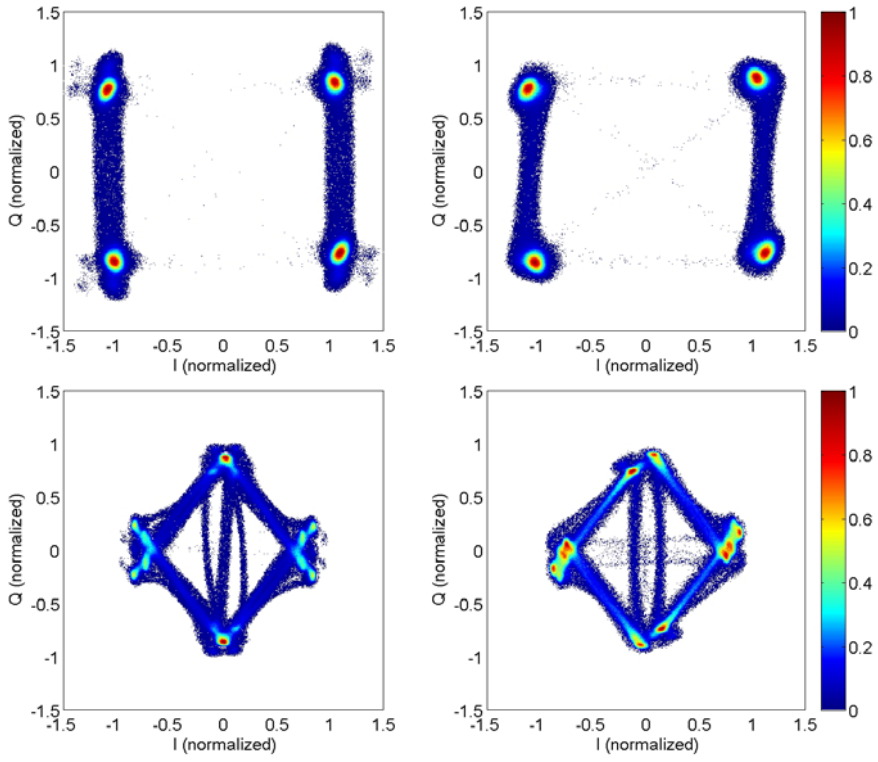

Fig. 6: IQ constellation diagrams for SVN49 at 40° elevation (left) and 90° elevation (right). The top plot depicts C/A- and P-code modulation on 16 April 2010, the bottom plot shows C/A-, Y- and M-code modulation on April 22, 2010. The effect of the reflected signal is clearly visible in the distortion of the diagram for high elevations.

In order to determine the characteristic parameters of the multipath, the measured samples used to generate the IQ constellation diagram at 40° elevation are taken as a reference and merged with a replica of this signal, which has been attenuated, delayed in time and shifted in phase. Then a constellation diagram is produced from the modified signal and correlated to the measured counterpart at high elevation. This procedure is repeated and the attenuation, delay and phase shift are varied over a predefined search space until the simulated constellation diagram with the highest correlation to the measured diagram is found (Thölert et al. 2009b).

The plots in Fig. 7 show the estimation for delay τ, attenuation α and phase shift φ of the observed multi-path of SVN49 for L1 and L2. The results are based on IQ samples of 5 ms length and taken every 10° elevation. Measurements from April 14, 15 and 22, 2010 have been processed. For each day, the ascending and descending part of the pass have been processed separately, resulting in two data points for each day. The estimated parameters exhibit a significant scatter, especially for lower elevations. This effect could be expected since the reflected signal is transmitted with lower power at low elevations and is thus more difficult to separate from noise and other errors. It should furthermore be noted that no estimations are provided for elevations of 40° for L1 and 30° for L2. The null of the gain pattern for the signals from the J2 port makes the multipath-component unobservable at the corresponding elevation angles.

Based on the estimations at high elevation angles, the delay can be approximated to about 41 ns for L1 and 40 ns for L2. According to the multipath model in Eq. 6a, the delay should stay constant over the complete range of elevations. Instead, significant variations in the order of several tens of nanoseconds are visible for lower elevations on L1 and L2. The estimates of the power ratio yield consistent results for elevations higher than 60°. At zenith, the power ratio of the signal reflection is approximately -15 dB on L1 and -23 dB on L2. It varies over elevation governed by the different boresight-dependent gain patterns of the signals from the J1 and J2-port. The estimates of the phase-shift exhibit only comparably little scatter over the entire range of elevations. At zenith, the L1 phase-shift amounts to 30°. It varies over elevation due to the variation in the relative phase of the signal from the two antenna ports. At elevations lower than 30°, the maximum scatter between the different estimates is on the order of 20°. For L2, the zenith phase-shift is approximately 75°. The maximum scatter at low elevation is on the order of 40°.

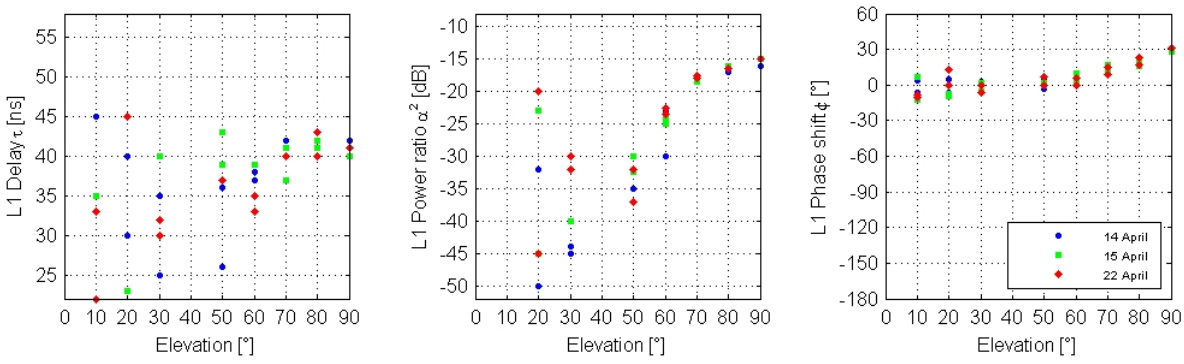

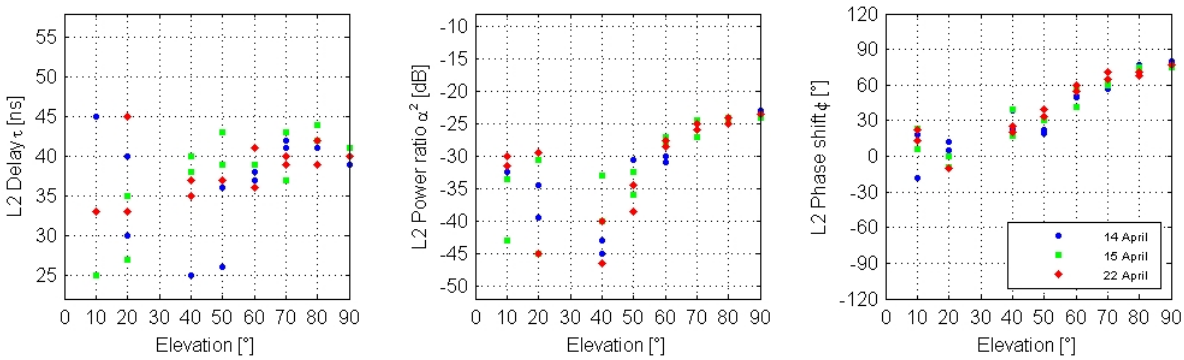

Fig. 7: SVN49 multi-path parameters over elevation estimated based on IQ-Method for L1 (top plots) and L2 (bottom plots). Plots depict delay, attenuation (expressed as power ratio) and phase shift from left to right for April 14, 15 and 22, 2010.

Summary and Conclusions

This paper provides an overview of the tracking campaign of SVN49 for an analysis of the satellite's internal signal reflection. DLR's 30 m dish antenna has been used to track passes with elevations higher than 89°. Measurements have been collected with a set of receivers to assess the impact of the satellite's internal signal reflection on the tracking using different correlator implementations. Due to the high directivity of the deep space antenna, local multipath errors are virtually eliminated and the high antenna gain allows tracking with high signal-to-noise ratios over the entire range of elevations from less than 5° up to zenith. The multipath combination of signals on different frequencies has been analyzed. For C/A code tracking on L1 with conventional early-minus-late correlators with 1.0 chip spacing, the multipath error reaches from -0.25 m at 5° elevation to 1.7 m at zenith, when normalizing the curve to zero at 40° elevation. For L2C code, the plot of the multipath combination over elevation has a different shape. It starts at about 0.2 m for low elevations, reaches -0.4 m for 65° elevation and amounts to -0.25 m at zenith. As expected, the impact of the signal reflection is reduced for narrow correlators. The repeatability of the results has been analyzed using tracking data from five satellite passes. Whereas the passes of the three middle days are consistent, the first and the last day of the test period exhibit notable deviations.

Receiver- or satellite-dependent effects can be responsible for these deviations. A variation of the multipath effect depending on the observation geometry could be expected caused by the gain patter variation due to the effect of the different antenna elements. However, from the satellite's perspective, the passes of the tracking campaign follow similar paths in the boresight-azimuth-diagram. Furthermore, a satellite-dependent effect would be observed by all receivers in a similar manner. However, the Javad receiver with 0.1 chip spacing exhibits very consistent results for the same test period. Taking all this into account, a receiver dependent effect appears more likely, but a conclusive statement is difficult to make at this point. As a complementary analysis to the tracking with the conventional early-minus-late correlator, tracking has also been performed with special correlators designed to mitigate multipath. Depending on the correlator design, the multipath induces by the signal reflection can be partially or completely mitigated.

The last results presented in this part of the paper are results from a technique to determine delay, phase shift and attenuation of the reflection based on an iterative correlation of measured and simulated IQ constellation diagrams. As a first approximation, the reflected signal on L1 is delayed by 41 ns. At zenith, the observed multipath is attenuated by -15 dB and shifted by 30° in phase. For L2, the delay amount to about 40 ns and the power ratio and phase shift at zenith are -23 dB and 75°, respectively.

The second part of this paper will present results for the chip shape reconstructed with from the IQ samples and from vision correlator measurements with the OEMV receiver. Finally, a multipath model will be derived to simulate the results for the different early-minus-late correlators obtained from the receiver tracking.

References

El-Arini MB, Conker RS, O'Laughlin DG, Hegarty CJ (2010) Effect of SVN49 (PRN01) on Position and Time Accuracy for Single-and Dual-Frequency Users. Proceedings of ION-GNSS-2010, 21-24 September 2010, Portland Oregon, USA

Ericson S, Shallberg K, Edgar C (2010) Characterization and Simulation of SVN49 (PRN01) Elevation Dependent Measurement Biases. Proceedings of ION ITM 2010, 25-27 January 2010, San Diego, California, USA

Erwin B, Irvine J, McFadden M, Powell T, Marquis W (2009) L5 Demo Payload. GPS World, May 2009, pp. 27-31

Gao GX, Heng L, De Lorenzo D, Lo S, Akos D, Chen A, Walter T, Enge P, Parkinson B (2009) Modernization Milestone – Observing the First GPS Satellite with an L5 Payload. InsideGNSS, May/June 2009, pp. 30-36

Hatch R, Knight J, Dai L (2007) Recent GNSS Developments at NavCom Technology. Proceedings of International Global Navigation Satellite Systems Society (IGNSS) Symposium, 4-6 December 2007, Sydney, Australia

Jones J, Fenton P, Smith B (2004) Theory and performance of the Pulse Aperture Correlator. available at http://www.novatel.com/Documents/Papers/PAC.pdf

Kee C, Parkinson B (1994) Calibration of multipath errors on GPS pseudorange measurements. In Proceedings of the 7th International Technical Meeting of the Satellite Division of the Institute of Navigation, Salt Lake City, UT, September 20-23 1994, pp.353 – 362

Komjathy A, Wilson BD, Mannucci AJ (2010) New developments on estimating satellite interfrequency bias for SVN49. GPS Solutions. DOI 10.1007/s10291-010-0185-5

Langley RB (2009) Expert Advice: Cause Identified for Pseudorange Error from New GPS Satellite SVN49. GPS World, August 2009, pp. 8-12

Meurer M, Erker S, Thölert S, Montenbruck O, Hauschild A, Langley RB (2009) GPS L5 First Light, GPS World, June 2009, pp. 49-59

Sleewaegen JM, Boom F (2001) Mitigating Short-Delay Multipath: a Promising New Technique, Proceedings of ION GPS 2001, 11-14 September 2001, Salt Lake City, Utah, USA

Springer T, Dilssner F (2009) SVN49 and other GPS Anomalies, InsideGNSS July/August 2009. pp. 32-36

Stansell T (LtCol Lake GPSW POC) (2009) briefing charts entitled: SVN-49 Signal Anomaly, Summary Report of the 49th Civil GPS Service Interface Committee (CGSIC), 21 September

Thölert S, Erker S, Montenbruck O, Hauschild A, Meurer M (2009a) GPS SVN49 - L1 Anomaly Analysis based on Measurements with a High Gain Antenna, 4th European Workshop on GNSS Signals and Signal Processsing, Oberpfaffenhofen

Thölert S., Erker S., Meuer M. (2009b); GNSS Signal Verification with a High Gain Antenna - Calibration Strategies and High Quality Signal Assessment; ION ITM 2009; 26-28 January 2009; Anaheim, California